coatings

MDPI

Article

Phosphonic Acid-Derived Dual-Metal Passivation of Cu and Al for Corrosion-Resistant Wire-Bonded Interconnects

Shinoj Sridharan Nair [1], Dinesh Kumar Kumaravel [1], Pavan Singh Ahluwalia [2], Khanh Tuyet Anh Tran [1], Duwage Anushka Sandaruwan Perera [1], Shyam Muralidharan Nair [1] and Oliver Chyan [1,*]

[1] Department of Chemistry, University of North Texas, Denton, TX 76201, USA; shinojnair@my.unt.edu (S.S.N.); dineshkumarkumaravel@my.unt.edu (D.K.K.); khanhtran5@my.unt.edu (K.T.A.T.); anushkaperera@my.unt.edu (D.A.S.P.); shyamnair@my.unt.edu (S.M.N.)
[2] Texas Academy of Mathematics and Science, University of North Texas, Denton, TX 76201, USA; pavanahluwalia@my.unt.edu
* Correspondence: oliverm.chyan@unt.edu; Tel.: +1-(940)-565-3463

Abstract

Copper–aluminum (Cu-Al) wire-bonded devices are widely used in microelectronic packaging; however, corrosion at exposed Cu-Al bimetallic interfaces can lead to Al pad degradation, undercutting, and eventual ball-bond lift-off or open-circuit failure under humid, halide-contaminated conditions. This work presents a scalable post-wire-bond wet-chemical passivation process using octadecylphosphonic acid (ODPA) to simultaneously modify exposed Cu/Pd-coated Cu (PCC) and Al surfaces. The passivation process includes a hydroxylation pretreatment to generate reactive oxide/hydroxide surface sites, followed by ODPA treatment and solvent rinsing to remove weakly adsorbed species. Surface modification was evaluated using contact-angle measurements, reflection–absorption infrared spectroscopy (RAIRS), atomic force microscopy (AFM), and X-ray photoelectron spectroscopy (XPS). ODPA treatment increased the water contact angle on Cu and Al, confirming a substantial increase in surface hydrophobicity following coating formation. RAIRS identified ODPA-associated aliphatic C-H bands, AFM showed treatment-induced nanoscale surface changes, and XPS supported metal–oxygen–phosphorus interfacial bonding. Under aggressive 100 ppm chloride-ion immersion, ODPA passivation strongly suppressed corrosion-induced ball-bond lift-off across both device platforms. Lift-off decreased from 99.0% to 0.73% for Cu-Al devices and from 23.3% to 0.42% for PCC-Al devices. Collectively, these findings establish an effective, process-compatible post-wire-bond strategy for substantially protecting corrosion-susceptible interfaces and thereby improving the reliability of wire-bonded interconnects in halide-containing environments.

Keywords: Cu-Al wire bonding; dual-metal passivation; octadecylphosphonic acid (ODPA); bimetallic corrosion; chloride-induced ball-bond lift-off

Check for updates

Academic Editor: Tadeusz Hryniewicz

Received: 13 June 2026
Revised: 14 July 2026
Accepted: 17 July 2026
Published: 18 July 2026

Copyright: © 2026 by the authors. Licensee MDPI, Basel, Switzerland. This article is an open access article distributed under the terms and conditions of the Creative Commons Attribution (CC BY) license.

1. Introduction

Wire bonding remains one of the most mature and extensively adopted interconnect technologies in microelectronics packaging, owing to its combination of low cost, high throughput, and broad compatibility with diverse device architectures. Although flip-chip, wafer-level, and heterogeneous integration technologies are becoming more common, wire bonding remains the preferred choice for high-volume manufacturing. It is still widely used in power, analog, memory, and mixed-signal devices [1–3]. At the same time, increasingly strict reliability requirements for automotive and other safety-critical electronics have made

near-zero-defect performance, often measured in defective parts per billion (DPPB), an essential target [4].

In response to these demands, copper (Cu) has largely replaced gold (Au) as the preferred wire-bonding material. Compared with Au, Cu is less expensive, provides better electrical and thermal conductivity [1,3], and forms Cu-Al intermetallic compounds more slowly at the bonding interface [5]. Despite these advantages, Cu-Al wire bonds remain susceptible to corrosion in humid environments containing mobile ionic contaminants [6]. One of the main consequences is corrosion-induced ball-bond lift-off, which can result in intermittent or complete open-circuit failure. These failures are commonly observed after humidity-based reliability tests, such as temperature–humidity bias (THB), pressure cooker testing (PCT), and highly accelerated stress testing (HAST), and are often associated with halide contamination [7]. Figure 1 shows representative SEM images of the failure progression, from an intact ball bond to Al bond-pad corrosion and eventual ball-bond lift-off under chloride exposure.

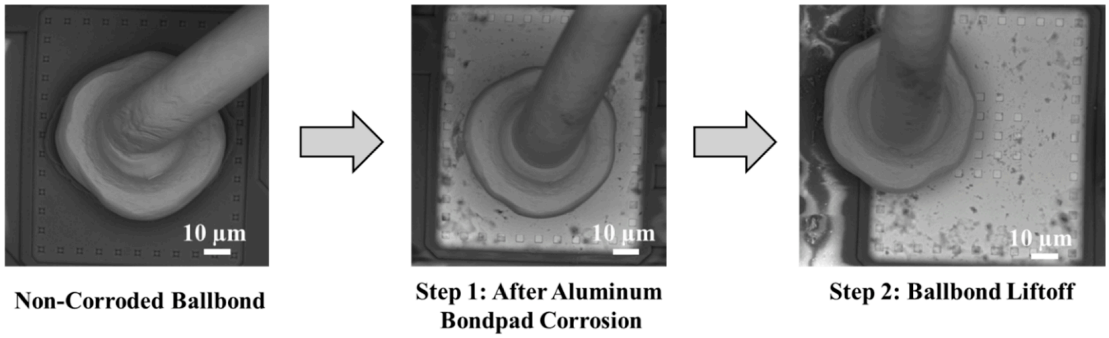

Figure 1. SEM (BED) images of ball bond before corrosion, after Al bond-pad corrosion, and after ball-bond lift-off.

This type of degradation can occur even when the halide concentration is relatively low. Previous studies on Cu-Al wire bonds have shown that chloride concentrations ranging from 5 to 20 parts per million can cause severe corrosion in the presence of moisture [4,8]. These chloride-containing impurities may originate from epoxy molding compounds (EMCs), adhesion promoters, additives, processing residues, or opportunistic manufacturing contamination [8,9]. Once moisture is present, the ions can become mobile and migrate toward exposed regions around the Cu-Al bond perimeter, where localized corrosion may begin. This sensitivity to trace ionic contamination remains a major challenge for long-term package reliability. To accelerate the evaluation and clearly distinguish between untreated and passivated devices, the present study uses a 100 ppm Cl^- aqueous solution as a deliberately severe screening condition. Under this condition, nearly all untreated Cu-Al devices undergo corrosion within the selected test duration, providing a stringent baseline against which the protective effectiveness of the coating can be directly compared. The 100 ppm concentration is not intended to represent the actual chloride level or transport conditions inside an encapsulated package. Instead, it provides a controlled and accelerated environment for evaluating the relative corrosion resistance of unprotected and passivated wire-bond assemblies.

The susceptibility of the Cu-Al system is fundamentally electrochemical, although the dominant corrosion pathway depends on the local Cu-Al phase composition, passive-film stability, chloride concentration, solution pH, and the extent of electrolyte access to the bimetallic interface [10–13]. Under high-temperature and high-humidity package-reliability stress tests, previous studies have reported preferential degradation of Cu-rich Cu-Al intermetallic compounds (IMCs) [6,14]. In contrast, real-time corrosion studies

indicate that halide-induced wire-bond failure can initiate at the electrolyte-accessible Cu-Al bond perimeter and then progress through localized Al-pad corrosion and undercutting toward the underlying IMC-containing region [4,11]. Under the room-temperature, 100 ppm Cl^- aqueous screening condition used in this study, chloride can destabilize the native Al oxide/hydroxide film and promote localized Al dissolution, while adjacent Cu/PCC surfaces and other accessible Cu-rich regions support coupled cathodic reactions. This localized bimetallic corrosion can propagate laterally beneath the ball bond, leading to Al-pad undercutting, eventual ball-bond lift-off, and, if the attack continues, subsequent degradation of the underlying IMC-containing region [4,11]. The dual-metal passivation strategy developed in this work is therefore intended to suppress corrosion at this accessible initiation site by modifying both the Al-containing and Cu/PCC-containing surfaces near the bond perimeter, thereby limiting early-stage corrosion before it can advance toward buried IMC-containing regions.

One widely adopted manufacturing approach for improving Cu-Al bond reliability is the use of palladium-coated copper (PCC) wire. The Pd coating can alter interfacial reactions, suppress the formation of highly corrosion-susceptible Cu-rich IMCs, and reduce direct exposure of reactive Cu; as a result, PCC-Al devices generally show better corrosion resistance than bare Cu-Al devices [14]. Nevertheless, PCC does not completely eliminate the Cu-Al galvanic couple. During free-air-ball formation and thermosonic bonding, the Pd coating may become non-uniform or discontinuous, while Al splash or squeeze-out can create exposed Cu-Al contact around the bond perimeter. PCC-Al devices can therefore still undergo corrosion and lift-off under aggressive halide exposure [4,15]. To evaluate the proposed treatment across both conventional and improved wire metallurgies, this study examines Cu-Al Low-Profile Quad Flat Package (LQFP) devices and PCC-Al Mold Array Process Ball Grid Array Package (MAPBGA) devices, as shown in Figure 2.

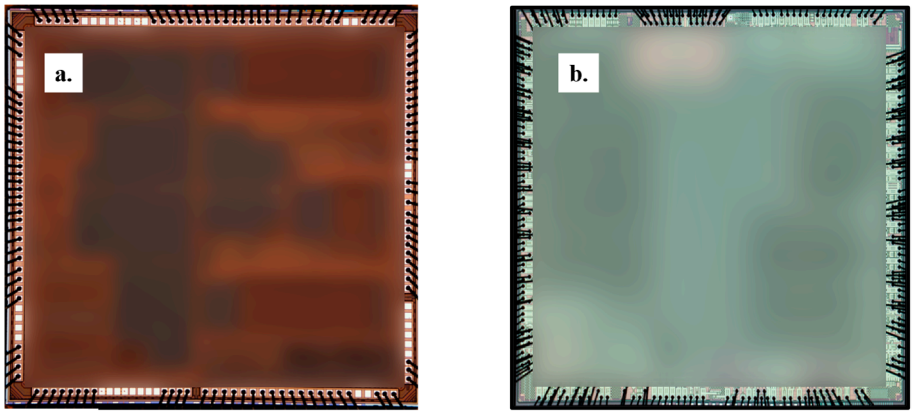

Figure 2. Optical microscope images of (**a**) LQFP (Cu-Al device) and (**b**) MAPBGA (PCC-Al device) devices used in the study.

Taken together, these limitations and the current understanding of the corrosion mechanism suggest that approaches focused only on wire metallurgy or IMC control may not be sufficient to protect the exposed Cu-Al bond perimeter. The exposed Cu/PCC-Al bimetallic contact at the bond perimeter is a primary site for corrosion initiation because electrolyte access enables galvanic reactions to occur between the Cu-containing surface and the adjacent Al [11,16]. Buried Cu-Al intermetallic phases may then influence how the corrosion progresses. Cu-selective passivation can reduce the reactivity of exposed Cu-containing regions, but it leaves the adjacent Al surface untreated [17]. As a result, it does not provide simultaneous protection to both sides of the Cu-Al galvanic couple in a completed wire-bonded device.

The present work advances corrosion-mitigation strategies by introducing a hydroxylation-assisted ODPA treatment that modifies Cu/PCC and Al surfaces after wire bonding. The treatment creates a hydrophobic bond-perimeter environment, where electrolyte access can promote coupled corrosion reactions [11,16]. Unlike approaches based only on Pd-containing wire metallurgy or Cu-selective passivation [14,17], this dual-metal strategy targets both sides of the Cu-Al galvanic couple in completed devices. The process avoids high-temperature post-treatment [18]. ODPA was selected because phosphonic acids bind strongly to metal oxide and hydroxide surfaces through M-O-P linkages [19]. Its C18 chain promotes a hydrophobic layer that can limit water and ion access. Here, the coating is better described as a heterogeneous phosphonate-derived layer with multilayered regions rather than an ideal monolayer. Depending on surface chemistry, phosphonate groups may adopt mono-, bi-, or tridentate coordination [20]. On Al oxide/hydroxide surfaces, ODPA can form chemisorbed and Al-phosphonate species [21], increasing hydrophobicity and reducing electrolyte access [22]. It can also form phosphonate-derived coatings on oxidized Cu, including CuO, $Cu(OH)_2$, and Cu_2O [23]. By modifying both metals, the treatment is expected to slow bond-perimeter corrosion. Figure 3 summarizes the proposed passivation mechanism.

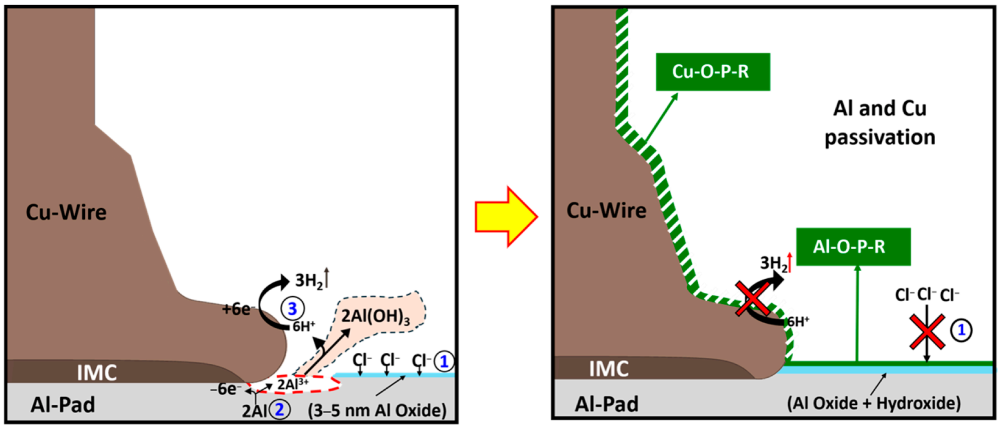

Figure 3. Schematic of corrosion mechanism and ODPA-assisted dual-metal passivation at Cu-Al bimetallic contacts in wire-bonded packages. The red crosses denote suppression of electrolyte access and the associated corrosion reactions following formation of the Cu-O-P-R and Al-O-P-R passivation layers.

Guided by this mechanism, the study evaluates a scalable wet process in which hydroxylation generates reactive oxide/hydroxide sites before ODPA exposure [24]. Surface modification was examined by contact-angle measurements, RAIRS, AFM, and XPS, consistent with studies of phosphonic-acid-treated Cu and Al surfaces [23,25]. Device performance was assessed by chloride-immersion screening of Cu-Al and PCC-Al assemblies. To our knowledge, this is the first demonstration of phosphonic-acid-based dual-metal passivation suppressing chloride-induced Al-pad degradation and ball-bond lift-off in devices.

2. Materials and Methods

2.1. Wire-Bonded Devices

Two types of wire-bonded package assemblies are used in this study. The first device type consisted of functional dies (5.0 mm × 4.6 mm) surface-mounted on Cu-based lead frames from low-profile quad flat packages (LQFP). These devices employed Cu wires (~25 µm diameter) thermosonically ball-bonded onto Al bond pads (70 µm × 78 µm). Throughout this manuscript, these assemblies are referred to as Cu-Al devices.

The second device type consisted of dies (~5.5 mm × 5.5 mm) surface-mounted on lead frames from mold array process ball grid array (MAPBGA) packages. These devices used Pd-coated Cu (PCC) wires (~20 μm diameter) for ball bonding and are referred to as PCC-Al devices.

2.2. Dual-Metal Passivation Process

A scalable wet-process dual-metal molecular passivation strategy was applied to Cu and Al wafers as well as Cu-Al and PCC-Al wire-bonded devices. All wafers and devices were used as received from our industrial collaborators. The process consisted of a controlled hydroxylation pretreatment followed by ODPA treatment.

First, the wafers or wire-bonded devices were immersed in 5 mM aqueous NaOH (pH ~11) for 2 min to activate the exposed Cu/PCC and Al-based surfaces. Immediately after the NaOH treatment, the samples were immersed in ultrapure water (UPW) at 70 °C for 10 min. This NaOH/UPW sequence was designed to promote the formation of hydroxylated oxide/oxyhydroxide surface sites prior to ODPA exposure. The approach was adapted from alkali-assisted Al surface-modification procedures in which dilute NaOH treatment followed by hot-water exposure generated an $Al(OH)_3$-rich surface layer [26]. In the present work, the milder 70 °C UPW treatment was used to promote surface hydroxylation rather than to intentionally form a thick hydroxide film.

Following the hydroxylation pretreatment, the samples were immersed for 1 h, unless otherwise specified, in a 1 mM octadecylphosphonic acid (ODPA) solution (pH ~4) prepared in ethanol (ODPA from MilliporeSigma, Burlington, MA, USA). The ODPA concentration was selected based on previous studies reporting ODPA-derived surface modification of Cu from 1 mM ethanolic solutions [23,27]. The hydroxylated oxide/oxyhydroxide surface sites are expected to facilitate ODPA attachment through interfacial metal–O–P bonding. After ODPA treatment, the samples were thoroughly rinsed with ethanol to remove weakly bound or physisorbed material, then dried under a nitrogen stream before characterization and corrosion screening.

The 1 h ODPA immersion time was selected through preliminary coating-time screening using PCC-Al devices. ODPA treatments of 10 min, 30 min, 1 h, 6 h, and 24 h were evaluated under the same chloride-immersion screening conditions. The 1 h treatment strongly suppressed corrosion-induced lift-off. Although the longer 6 h and 24 h treatments also provided effective protection, they did not offer a practical advantage over the 1 h condition that would justify the substantially longer processing times. In contrast, the 10 min and 30 min treatments were less effective than the 1 h condition. Therefore, 1 h was selected as a practical balance between corrosion mitigation and process duration for potential microelectronics-packaging applications. The corresponding coating-time screening results are provided in Table S1.

2.3. RAIRS and Wettability

RAIRS was performed using a Thermo-Nicolet iS50 (Madison, WI, USA) spectrometer to verify adsorption of octadecylphosphonic acid species via characteristic aliphatic C-H stretching signatures and to assess relative film coverage across samples. Spectra were collected on representative treated and untreated surfaces under consistent acquisition conditions.

Static water contact-angle measurements were used to quantify wettability changes after ODPA treatment. Measurements were performed using a YSC M400 power scope (Fremont, CA, USA) by dispensing 10 μL UPW droplets onto passivated and control wafer surfaces. Droplet images were analyzed using ImageJ (Version 1.54g), and contact angles were reported as the mean ± standard deviation.

2.4. Atomic Force Microscopy (AFM)

Surface topography changes resulting from passivation were examined using a Park NX10 atomic force microscope (Gwacheon-si, Gyeonggi-do, Republic of Korea). Images were collected in non-contact mode with PPP-NCHR cantilevers to minimize tip-sample interactions and reduce the likelihood of disturbing the ODPA-derived surface layer. For each condition, four independently selected scan areas were analyzed to assess surface morphology and determine the average roughness (Sa) and root-mean-square roughness (Sq). The reported roughness values are presented as the mean ± standard deviation from these four measurements. The approximate thickness of the ODPA-derived coating on Cu was estimated by creating localized boundaries between coated and stripped regions on ODPA-treated Cu wafers. Selected areas were exposed to 3.5% sulfuric acid to remove the surface coating locally. Step-height profiles were then acquired across the resulting boundaries by comparing relatively flat coated and stripped regions while avoiding isolated large surface features. Measurements were collected at three independently selected locations and are reported as the mean ± standard deviation. All AFM data were processed using Park Systems XEI software (version 5.2.0) with the same plane-subtraction and analysis settings applied across all samples.

2.5. SEM Imaging and XPS Analysis

Scanning electron microscopy (SEM) was used to examine the wire-bonded devices at key stages of the corrosion screening process. Images were acquired using a JEOL IT200 microscope (Akishima, Tokyo, Japan) operated at 5 kV. A backscattered electron detector (BED-C, composition mode) was used to provide compositional contrast and clearly resolve corrosion features around the bond perimeter.

X-ray photoelectron spectroscopy (XPS) was performed on passivated Al and Cu wafer samples using a PHI 5000 VersaProbe scanning XPS microprobe (Physical Electronics, Chanhassen, MN, USA) equipped with an Al Kα source. Measurements were collected at an anode voltage of 11 kV and a pass energy of 29.35 eV. For both Al-ODPA and Cu-ODPA samples, the binding-energy scale was charge-referenced to the C 1s peak at 284.8 eV. Spectra were processed using CasaXPS software (Version 2.3.26PR1.0).

2.6. Accelerated Immersion Corrosion Screening Metrology

Accelerated corrosion screening was performed using aqueous chloride solutions prepared in ultrapure water (UPW; 18.2 MΩ·cm resistivity; EQ-7008 system, MilliporeSigma, Burlington, MA, USA). The screening solution contained 100 ppm chloride and was prepared using ACS-grade sodium chloride (EMD Millipore, Billerica, MA, USA). The resulting solution had a pH of approximately 5.

Wire-bonded devices were fully immersed in the 100 ppm Cl^- solution for 2 h under ambient atmospheric conditions. Chloride was selected as the primary screening ion because it is commonly associated with packaging contamination and can aggressively destabilize the native Al oxide/hydroxide layer at exposed Cu-Al bond perimeters. Evaluation under mixed-halide conditions is reserved for future reliability studies.

Corrosion initiation and progression were monitored in real time using a Nikon Eclipse LV150N optical microscope (Nikon Instruments Inc., Melville, NY, USA) equipped with a DS-Ri2 camera (Nikon Instruments Inc., Melville, NY, USA). Time-dependent images were collected at defined intervals to track morphological changes around the ball-bond perimeter and relate the observed corrosion damage to the final failure outcome [11].

Device reliability was quantified using ball-bond lift-off as the failure criterion. The percentage of lifted bonds was calculated as

$$\% \text{ Lift-off} = (N_{lifted}/N_{total}) \times 100,$$

where N_{lifted} is the number of wire bonds exhibiting lift-off, and N_{total} is the total number of wire bonds in a PCC-Al or Cu-Al device. Failure statistics and plots were generated in Origin (Version 2025b). The real-time immersion corrosion-screening setup, in which the Cu-Al or PCC-Al device is fully immersed in 100 ppm Cl^- solution and monitored under an optical microscope, is illustrated in Figure 4.

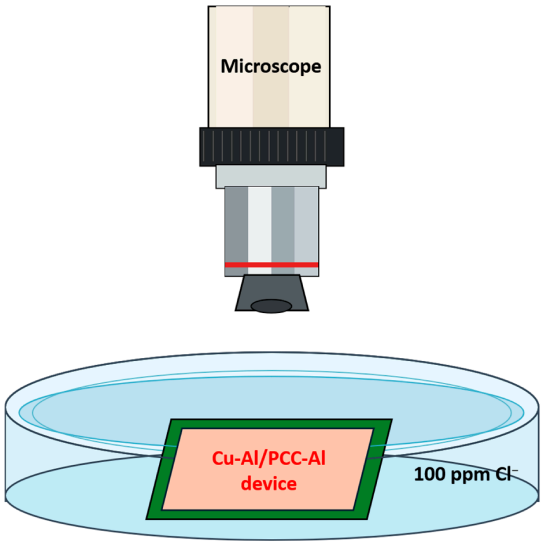

Figure 4. Schematic of real-time corrosion screening of Cu-Al and PCC-Al devices in a 100 ppm Cl^- solution for 2 h, monitored in situ by optical microscopy.

3. Results and Discussion

3.1. Changes in Surface Wettability

Contact-angle measurements were used to evaluate the effect of ODPA treatment on the wettability of Al and Cu surfaces (Figure 5). Before passivation, the Al surfaces exhibited water contact angles ranging from 80.7° to 84.5° (mean: 82.7°). Following ODPA treatment, the contact angles increased to 115.4–124.0° (mean: 119.1°), indicating a substantial decrease in wettability and a transition to a more hydrophobic surface [22,25,28]. A similar trend was observed for Cu. The untreated Cu samples exhibited contact angles ranging from 61.7° to 69.5° (mean: 65.3°), whereas the ODPA-treated Cu samples showed values of 90.2–95.0° (mean: 92.9°) [23].

The consistent increase in water contact angle on both Al and Cu indicates that ODPA treatment altered the surface chemistry of both components of the Cu-Al galvanic couple, creating a more hydrophobic interfacial environment. When considered together with the XPS and RAIRS results, this wettability change is consistent with the formation of an ODPA-derived layer in which phosphonate groups interact with hydroxylated metal oxide sites, and the C18 alkyl chains preferentially extend away from the surface [22,23]. At exposed Cu-Al regions near the ball-bond perimeter, the lower wettability may reduce the residence and accessibility of the chloride-containing aqueous electrolyte. Because chloride-induced corrosion requires electrolyte access to initiate localized anodic dissolution and coupled cathodic reactions, the increased hydrophobicity is consistent with the reduced Al-pad undercutting and ball-bond lift-off observed after ODPA treatment. However, the contact-angle measurements do not directly quantify water uptake, chloride transport, or galvanic-current suppression at the wire-bond interface.

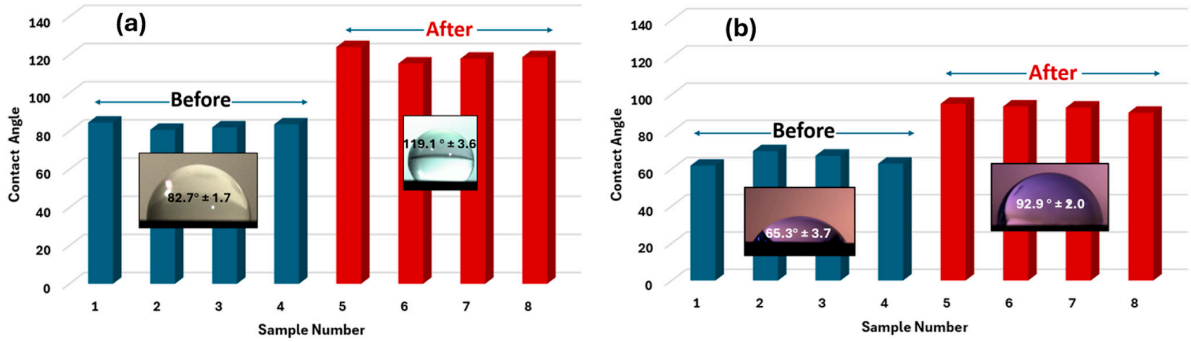

Figure 5. Contact angle analysis of (**a**) Al and (**b**) Cu wafers before and after ODPA passivation (number of wafers tested per condition = 4).

3.2. Chemical Bonding Signatures from RAIRS

Following the contact-angle measurements, RAIRS was used to confirm the chemical presence of the ODPA-derived layer on the hydroxylated Cu and Al surfaces, as shown in Figure 6. Relative to the hydroxylated controls, both ODPA-treated substrates show clear aliphatic C-H stretching bands in the 2800–3000 cm^{-1} region, confirming the presence of long-chain alkyl species associated with ODPA. For Al-ODPA, the asymmetric CH_2 and CH_3 stretching bands are observed at approximately 2918 and 2959 cm^{-1}, respectively, while the symmetric CH_2 stretch appears near 2850 cm^{-1} [29]. The Cu-ODPA surface shows corresponding bands at approximately 2850, 2917, and 2956 cm^{-1} [27]. A CH_2 bending/scissoring band near 1465 cm^{-1} provides further evidence of an ODPA-derived alkyl layer on both substrates [30].

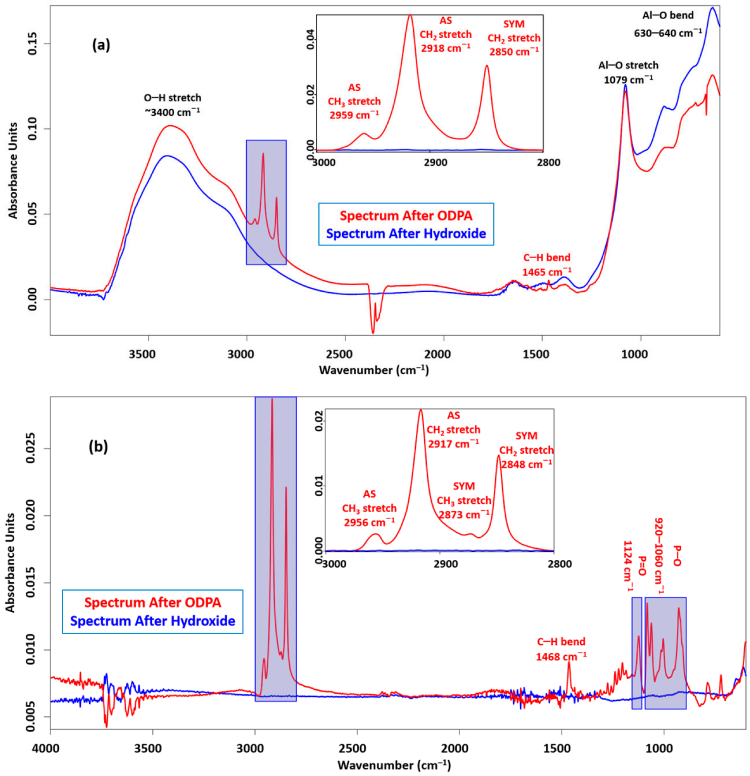

Figure 6. RAIRS spectra of (**a**) Al-ODPA and hydroxylated Al, and (**b**) Cu-ODPA and oxidized/hydroxylated Cu (AS, asymmetric; SYM, symmetric). The shaded regions highlight the spectral ranges containing characteristic ODPA-related C-H stretching and phosphonate-group vibrations.

For the Cu-ODPA sample, additional features appear in the lower-wavenumber region, particularly between approximately 1000 and 1150 cm^{-1}. These bands are assigned mainly to P-O stretching vibrations of surface-associated phosphonate groups, with possible contributions from P=O-related modes [31]. Their appearance after ODPA treatment, together with the aliphatic C-H bands, supports the formation of an ODPA-derived interfacial layer on the oxidized/hydroxylated Cu surface. Overall, the RAIRS results complement the contact-angle data by providing direct vibrational evidence of ODPA-derived alkyl and phosphonate species on the treated surfaces. When considered together with the other surface characterization results, these findings are consistent with the formation of a molecular coating that can reduce surface wettability and help limit electrolyte access in Cu-Al interconnect environments.

3.3. Analysis of Surface Morphology Using AFM

AFM was used to compare the surface morphology of Cu and Al wafers before and after ODPA treatment, as shown in Figure 7. The untreated substrates were not completely smooth and contained localized nanoscale variations associated with their growth or deposition processes. These features were retained in the roughness analysis because they represent the inherent substrate morphology.

The untreated electroplated Cu surface was relatively smooth, with *Sa* and *Sq* values of 1.2 ± 0.1 nm and 1.8 ± 0.2 nm, respectively. Sparse nanoscale protrusions were also observed and may be associated with local electroplating variations, such as growth-related nodules or asperities. Because these features were isolated, their contribution to the overall roughness remained limited.

Following ODPA treatment, the Cu surface became substantially more heterogeneous, with *Sa* and *Sq* increasing to 16.3 ± 2.0 nm and 24.6 ± 4.1 nm, respectively. The larger relative increase in *Sq* indicates that localized high-height features made a strong contribution to the overall height distribution. To estimate the thickness of the Cu-ODPA coating, selected regions were exposed to 3.5% sulfuric acid to create boundaries between coated and locally stripped areas. Dilute sulfuric acid was selected because protonation of the surface-bound phosphonate groups, together with dissolution of the underlying Cu oxide/hydroxide anchoring layer, promotes local removal of the ODPA-derived coating and creates a measurable coated-to-stripped boundary for AFM step-height analysis. Step-height profiles were collected at three independently selected locations across relatively flat regions, avoiding isolated tall features. The resulting average step height was 70.6 ± 7.6 nm. This value is interpreted as the approximate thickness of the heterogeneous ODPA-derived surface layer rather than that of a uniform molecular monolayer.

The untreated epitaxial Al surface showed a more heterogeneous baseline morphology than the Cu surface, with Sa and Sq values of 5.8 ± 1.8 nm and 7.3 ± 2.2 nm, respectively. This higher initial roughness could be related to the growth morphology of the epitaxial Al layer, including broader height variations and localized raised features. After ODPA treatment, Sa and Sq increased to 18.6 ± 1.0 nm and 23.5 ± 1.3 nm, respectively. The treated Al surface also exhibited a greater number and wider distribution of nanoscale features, which, together with the other surface-characterization results, is consistent with the formation of a dense ODPA-derived layer over the Al surface.

A direct AFM thickness measurement was not performed on Al because the sulfuric-acid stripping method used for Cu could alter the native Al oxide/hydroxide layer and locally etch the underlying metal due to the higher chemical reactivity of Al. Under those conditions, the measured step height would not represent the ODPA-derived coating alone. As an alternative, the RAIRS intensity was used as a semi-quantitative indicator of the relative amount of ODPA-derived material on the Al surface. The asymmetric CH_2

stretching band for Al-ODPA was approximately 50 mAbs, compared with approximately 20 mAbs for Cu-ODPA. In our previous Cu-selective passivation studies, RAIRS peak intensity was correlated with independently measured coating thickness using QCM and AFM data [17,18]. Applying the same approach and using the Cu-ODPA step height of 70.6 ± 7.6 nm as a reference, the Al-ODPA layer was estimated to be on the order of ~180 nm. This value should be regarded as an approximate estimate rather than a direct thickness measurement because a substrate-specific calibration was not established for Al-ODPA. Overall, the increase in roughness observed on both Cu and Al is consistent with substantial treatment-induced surface modification and the formation of heterogeneous ODPA-derived layers with locally raised, likely multilayered regions. Together with the RAIRS and other surface characterization results, the AFM data support the successful ODPA-based modification of both metal surfaces. Roughness values represent the mean of four independently analyzed regions for each condition, with the reported standard deviations indicating reasonable spatial reproducibility.

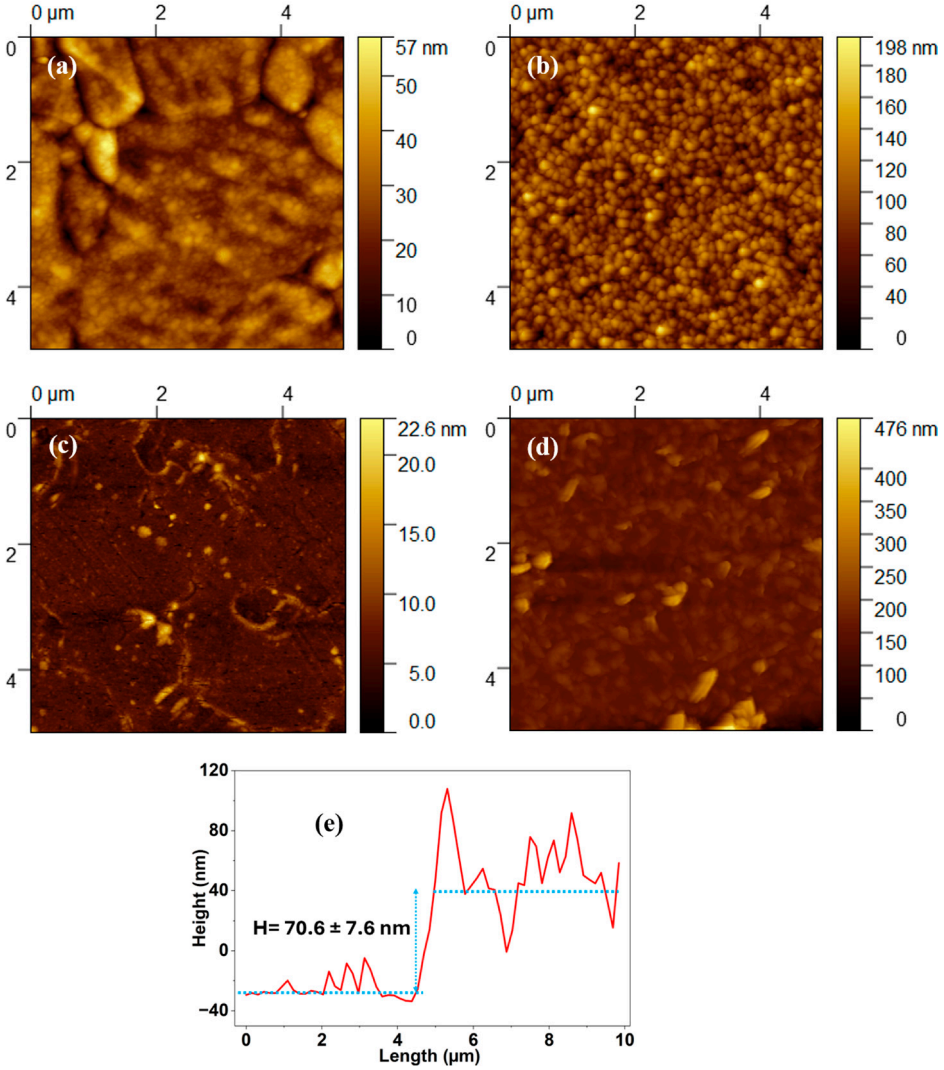

Figure 7. AFM topography images of untreated and ODPA-treated Al and Cu surfaces: (**a**) untreated Al, (**b**) ODPA-treated Al, (**c**) untreated Cu, and (**d**) ODPA-treated Cu. All images are analyzed across a 5 × 5 µm^2 area. (**e**) Representative AFM height profile across a boundary between ODPA-coated and locally sulfuric-acid-stripped Cu. Measurements at three independently selected locations gave an approximate Cu-ODPA film thickness of 70.6 ± 7.6 nm.

3.4. Chemical Bonding Analysis by XPS

X-ray photoelectron spectroscopy (XPS) was used to evaluate the surface chemistry of Al and Cu after hydroxylation pretreatment and subsequent ODPA passivation. XPS survey spectra of ODPA-passivated Cu and Al surfaces are provided in Figures S1 and S2, respectively, confirming the presence of P 2p signals together with C 1s and O 1s features before high-resolution peak analysis. Since ODPA attachment to oxidized or hydroxylated metal surfaces is expected to occur through interactions between the phosphonic acid headgroup and surface M-OH/M-O sites, high-resolution P 2p and O 1s spectra were collected to identify phosphorus incorporation and changes in the oxygen bonding environment. The P 2p region was used to verify the presence of ODPA-derived phosphonate species, while the O 1s region was analyzed to distinguish contributions from metal oxides/hydroxides and phosphonate-related oxygen environments. The observed peak positions and deconvoluted components provide surface-chemical evidence for ODPA functionalization on both Al and Cu, supporting the formation of molecular passivation layers relevant to corrosion mitigation.

3.4.1. Al-ODPA Thin Film

The Al-ODPA P 2p spectrum (Figure 8a) was deconvoluted into two phosphorus environments at 133.2 eV and 134.4 eV, with a residual standard deviation (STD) of 0.84. The major component at 133.2 eV, accounting for 71.0% of the total P 2p area, is assigned to chemically bound phosphonate species associated with interfacial Al-O-P bonding. The higher-binding-energy component at 134.4 eV, contributing 29.0%, is attributed to residual molecular phosphonic acid-like species, such as uncondensed -$CH_2P(O)(OH)_2$-containing environments [32]. This assignment is consistent with phosphonic acid adsorption on hydroxylated aluminum oxide surfaces, where condensation between surface Al-OH groups and phosphonic acid moieties can form interfacial Al-O-P linkages, while a fraction of non-condensed phosphonic acid groups may remain on the surface [22,33].

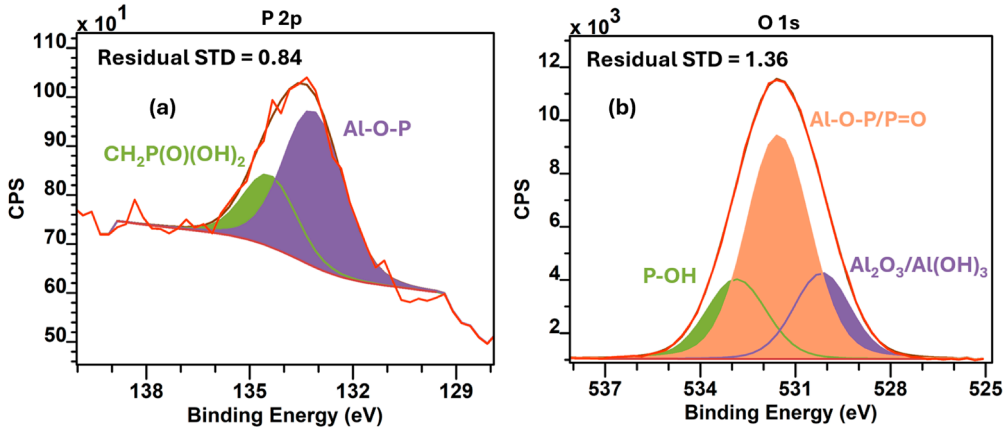

Figure 8. High-resolution XPS spectra of ODPA-coated Al wafers showing peak deconvolution of (**a**) P 2p and (**b**) O 1s regions into their respective chemical-state components (fits and residuals shown). Colored regions represent the deconvoluted components.

The O 1s spectrum (Figure 8b) was fitted with three components at 530.2 eV, 531.6 eV, and 532.9 eV, with a residual STD of 1.36. The low-binding-energy component at 530.2 eV is assigned to oxygen from the underlying aluminum oxide/hydroxide surface, including Al_2O_3 and $Al(OH)_3$-related species. The dominant component at 531.6 eV is assigned primarily to oxygen involved in Al-O-P bonding, with possible overlap from phosphoryl P=O and surface hydroxyl/oxide-related oxygen species [34–36]. The higher-binding-energy component at 532.9 eV is attributed to P-OH-related oxygen from incompletely

condensed phosphonic acid groups [36,37]. Together, the P 2p and O 1s spectra support the formation of a chemically anchored ODPA-derived layer on Al through interfacial Al-O-P bonding while also indicating the presence of a minor fraction of residual, uncondensed phosphonic acid functionality.

3.4.2. Cu-ODPA Thin Film

High-resolution XPS was used to characterize the Cu surface after ODPA treatment. The Cu-ODPA P 2p spectrum (Figure 9a) was deconvoluted into two phosphorus components at 133 eV and 134.4 eV, with a residual STD of 1.01. The major component at 133 eV, accounting for 70.2% of the total P 2p area, is assigned to chemically bound phosphonate species associated with interfacial Cu-O-P bonding. The higher-binding-energy component at 134.4 eV, contributing 29.8%, is attributed to residual molecular phosphonic acid-like phosphorus environments, such as incompletely condensed -$CH_2P(O)(OH)_2$ containing species [27,32,33,38]. This assignment is consistent with phosphonic acid adsorption on oxidized/hydroxylated metal oxide surfaces, where condensation between surface M-OH groups and phosphonic acid moieties can form interfacial M-O-P linkages, while a fraction of uncondensed phosphonic acid functionality may remain on the surface [32,33]. The O 1s spectrum (Figure 9b) was fitted with three oxygen components at 530.4 eV, 531.4 eV, and 532.6 eV, with a residual STD of 1.23. The low-binding-energy component at 530.4 eV is assigned to oxygen from native copper oxide/hydroxide species, represented as $CuO_x/Cu(OH)_x$. The dominant component at 531.4 eV is assigned primarily to oxygen involved in Cu-O-P bonding, with possible overlap from phosphoryl P=O oxygen [19,23,38]. The higher-binding-energy component at 532.6 eV is attributed to P-OH-related oxygen from incompletely condensed phosphonic acid groups [39,40]. Similar to that observed on the Al surface, the P 2p and O 1s spectra support the formation of a chemically anchored ODPA-derived layer on Cu through interfacial Cu-O-P bonding while also indicating the presence of a minor fraction of residual uncondensed phosphonic acid functionality.

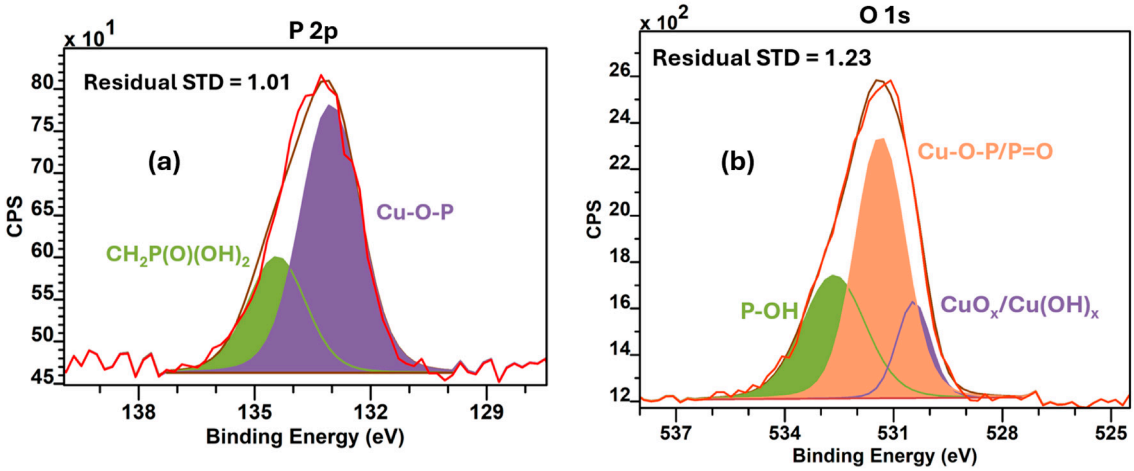

Figure 9. High-resolution XPS spectra of ODPA-coated Cu wafers showing peak deconvolution of (**a**) P 2p and (**b**) O 1s regions into their respective chemical-state components (fits and residuals shown). Colored regions represent the deconvoluted components.

Overall, the P 2p and O 1s XPS results support successful ODPA functionalization on both Al and Cu surfaces through interfacial M-O-P bonding [23,34,36]. The dominant lower-binding-energy P 2p components indicate chemically bound phosphonate species, while the higher-binding-energy P 2p components and P=O/P-OH-related O 1s contributions suggest the presence of residual, incompletely condensed phosphonic acid groups [22,32,33,38]. Therefore, the ODPA interface is unlikely to be exclusively tridentate and is more reasonably

described as a mixed mono-/bidentate metal–phosphonate coordination. Because O 1s signals from metal oxides/hydroxides, M-O-P, P=O, P-OH, and adventitious oxygen species can strongly overlap, exact component assignment should be interpreted cautiously and in combination with the P 2p results [36,40]. Altogether, these spectra provide surface-chemical evidence for chemically anchored ODPA-derived passivation layers on both Al and Cu.

3.5. Corrosion Screening Results for Wire-Bonded Devices

The corrosion-screening results in Figure 10 quantitatively distinguish the performance of the control and passivation-coated devices. Among the untreated controls, the Cu-Al devices exhibited nearly complete failure, with a wire-bond lift-off rate of 99.0%, confirming the high susceptibility of the conventional Cu-Al structure to chloride-induced Al-pad corrosion and subsequent bond lift-off [11]. The PCC-Al control devices showed improved resistance but still exhibited a substantial lift-off rate of 23.3%, indicating that the Pd coating mitigates, but does not eliminate, chloride-driven corrosion under the present high-halide screening condition [4,14]. Representative in situ, time-resolved optical micrographs of untreated PCC-Al control devices are provided in Figure S3. The highlighted bonds show the sequential failure process observed during chloride immersion: localized bubble formation near the bond perimeter, followed by progressive Al-pad corrosion and accumulation of dark corrosion products, and, ultimately, ball-bond lift-off. The bubble formation is consistent with cathodic hydrogen evolution on accessible Cu- or PCC-rich regions occurring concurrently with localized anodic dissolution of adjacent Al-containing regions [11]. In contrast, the SEM images in Figure 1 were acquired ex situ and show the corresponding corrosion-related morphological changes at the bond region after exposure. The ODPA-based passivation treatment nearly eliminated wire-bond lift-off for both device types, reducing the failure rate to 0.73% for Cu-Al devices and 0.42% for PCC-Al devices under the same 100 ppm Cl^- exposure. The time-resolved corrosion observations and quantitative lift-off data therefore demonstrate that the dual-metal passivation treatment effectively protects corrosion-susceptible regions at and near the bond perimeter. This suppression of Al-pad degradation and bond lift-off shows that the surface-level protection provided by the ODPA-derived coating translates into a substantial improvement in device-level reliability under aggressive chloride screening.

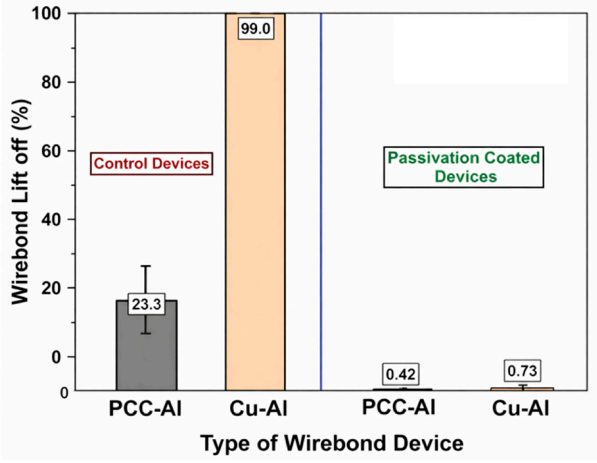

Figure 10. Wire-bond lift-off of untreated and ODPA-passivated PCC-Al and Cu-Al devices after 2 h immersion in 100 ppm Cl^- solution. The vertical blue line separates the control and passivated devices. ODPA treatment reduced lift-off from 23.3% to 0.42% for PCC-Al and from 99.0% to 0.73% for Cu-Al devices. n = 3 devices per condition; error bars represent standard deviation.

3.6. Mechanism of Passivation

The protection of both sides of the Cu-Al galvanic couple provides a plausible explanation for the corrosion-mitigation behavior observed during immersion screening. In untreated Cu-Al and PCC-Al devices, the chloride-containing electrolyte can reach the exposed bond perimeter, destabilize the Al oxide/hydroxide layer, and promote anodic Al dissolution. At the same time, the adjacent Cu or PCC surface can support cathodic reactions, including hydrogen evolution under locally acidic conditions [4,11,41]. This coupled electrochemical process accelerates Al-pad consumption and eventually leads to ball-bond lift-off [11,41].

Following ODPA treatment, the hydroxylated Cu- and Al-containing surfaces are converted into metal–phosphonate interfaces through M-O-P bonding, while the outward-oriented C-18 alkyl chains increase surface hydrophobicity and reduce electrolyte residence near the bond perimeter [22,23]. Optical images collected after extended ODPA treatment for 24 h show localized coloration or darkening near the ball-bond regions, which is consistent with ODPA-derived coating formation (Figure S4). The passivation layer is therefore expected to act through two complementary mechanisms: limiting water and halide access to anodic Al sites and reducing the availability of reactive cathodic sites on the Cu/PCC surface [11,17,23]. Together, these effects interrupt the galvanic corrosion pathway responsible for rapid Al dissolution and subsequent ball-bond lift-off. The marked reduction in lift-off after ODPA treatment is therefore attributed to a chemically anchored, hydrophobic molecular barrier rather than to a loosely deposited physical residue, consistent with the wettability, RAIRS, AFM, XPS, and device-level corrosion results [21–23].

Although the chloride-immersion results show substantial suppression of corrosion-induced lift-off at the device level, the present study does not directly quantify corrosion current, corrosion rate, or galvanic-current suppression. Conventional electrochemical measurements performed separately on planar Cu and Al coupons would not adequately represent the completed Cu/PCC-Al wire-bond structure because they would isolate the two metals and remove the localized bimetallic coupling, evolving anodic-to-cathodic area ratio, Cu-Al intermetallic-containing regions, bond-perimeter geometry, and confined electrolyte-access conditions that govern device failure. The corrosion-susceptible region in the wire-bonded device is a heterogeneous and continuously evolving assembly containing exposed Cu/PCC wire or ball surfaces, Al bond-pad material, Cu-Al intermetallic-containing regions, native oxides/hydroxides, and an electrolyte-accessible bond perimeter. During chloride exposure, Al-containing regions undergo localized anodic dissolution, while adjacent Cu/PCC and accessible Cu-rich regions support coupled cathodic reactions. As Al-pad undercutting progresses, the exposed areas, local electrolyte chemistry, and galvanic-current distribution change substantially. Accordingly, corrosion rates derived from separate Cu and Al coupons would not directly quantify the corrosion behavior of the coupled wire-bond system. Wire-bond lift-off percentage was therefore used as the device-relevant corrosion endpoint because it directly captures the practical failure mode of interest: chloride-induced bimetallic corrosion leading to Al-pad undercutting and loss of mechanical bond integrity.

The present chloride-immersion screening demonstrates that the hydroxylation-assisted ODPA treatment can mitigate acute corrosion-driven undercutting and lift-off, but it does not establish the full-service lifetime of the passivation layer in an encapsulated device. Chloride contamination from epoxy molding compounds is relevant at low ppm levels, and previous Cu-Al wire-bond corrosion studies have used 5–20 ppm Cl^- aqueous solutions at pH 5 to simulate EMC-related ionic contamination [8]. The 100 ppm Cl^- solution used in this work was therefore selected as an intentionally accelerated aqueous challenge rather than as a direct reproduction of the chloride concentration or transport

environment within an encapsulated package. Direct immersion is also more aggressive than the packaged environment because ionic transport in liquid water is substantially faster than through the solid EMC matrix.

The observed surface chemistry is consistent with phosphonate anchoring to hydroxylated Cu- and Al-oxide surfaces, and phosphonic-acid monolayers are generally reported to exhibit strong oxide binding and appreciable thermal stability. However, actual device operation may involve combined thermal, humidity, electrical bias, molding compound, and mechanical stresses that could alter coating coverage or integrity over extended periods. Future work should therefore evaluate coating retention and device-level protection after biased and unbiased HAST, high-temperature storage, thermal cycling, and prolonged humidity exposure, supported by post-aging surface characterization and standardized bond-integrity measurements. Future manufacturing-qualification studies should determine whether the treatment affects the mechanical integrity of finished wirebonds by performing wire-pull and ball-shear tests before and after treatment, as well as after relevant reliability stresses, to evaluate long-term durability. These studies will help define both the operational durability and manufacturing compatibility of the ODPA-assisted dual-metal passivation strategy.

4. Conclusions

This study demonstrates that hydroxylation-assisted ODPA treatment substantially improves the chloride-corrosion reliability of Cu-Al and PCC-Al wire-bond interconnects. By modifying exposed Cu/PCC- and Al-containing surfaces after bonding, the treatment forms a hydrophobic interfacial layer near the ball-bond perimeter. Contact-angle measurements confirmed increased hydrophobicity, while RAIRS and XPS provided evidence of ODPA-derived surface modification and metal–oxygen–phosphorus bonding. AFM further showed a heterogeneous, likely multilayered surface layer. Under 100 ppm Cl^- immersion, untreated Cu-Al and PCC-Al devices exhibited lift-off rates of 99.0% and 23.3%, respectively. After ODPA treatment, these values decreased to 0.73% and 0.42%, demonstrating suppression of chloride-induced Al-pad undercutting and ball-bond lift-off. Together, the surface characterization and device-level results are consistent with a chemically anchored, hydrophobic barrier that limits electrolyte access to vulnerable Cu-Al regions. However, water and halide transport and galvanic-current suppression were not directly quantified. The process, therefore, offers a scalable, process-compatible route for improving wire-bond reliability in halide-contaminated environments. Future work should address packaged-device validation, long-term coating stability, bond-integrity retention, metallurgy compatibility, and electrochemical behavior through biased and unbiased HAST, high-temperature storage, thermal cycling, prolonged humidity exposure, polarization, electrochemical impedance spectroscopy, and galvanic-current measurements.

Supplementary Materials: The following supporting information can be downloaded at https://www.mdpi.com/article/10.3390/coatings16070862/s1, Table S1. Effect of immersion time in 1 mM ODPA/EtOH following hydroxylation on the chloride-corrosion performance of PCC–Al devices, expressed as wire-bond lift-off percentage. The results were used to guide selection of the ODPA treatment duration. Although the lift-off percentage did not decrease strictly monotonically with immersion time, all treatments of 1 h or longer produced substantially lower failure rates than the 10 and 30 min treatments, indicating that sufficient immersion time is important for effective surface passivation. Figure S1. XPS survey spectrum of the ODPA-passivated Cu surface. The spectrum shows the presence of C 1s, O 1s, P 2p, and Cu 2p signals, along with Cu LMM Auger and C KLL features. The detection of phosphorus together with carbon and oxygen supports the presence of an ODPA-derived phosphonate layer on the Cu surface after passivation; Figure S2. XPS survey spectrum of the ODPA-passivated Al surface. The spectrum shows the presence of O 1s, C 1s, P 2p,

Al 2s, and Al 2p signals, along with an O KLL Auger feature. The detection of phosphorus together with carbon and oxygen supports the formation of an ODPA-derived phosphonate layer on the Al surface after passivation; Figure S3. Progressive bond-pad corrosion in control PCC-Al devices. Optical micrographs showing representative stages of corrosion development at selected Al bond pads connected to Pd-coated Cu wire bonds under chloride exposure. Red dashed boxes highlight the affected wire-bond/bond-pad regions, illustrating localized corrosion initiation, growth of dark corrosion products, and progressive degradation of the Al bond-pad interface in unpassivated control devices. Figure S4. Optical microscopy images of wire-bonded devices after ODPA passivation. The ODPA-coated devices show darkening around the ball-bond regions, indicating surface modification near the wire-bond area. In contrast, the surrounding Al bond-pad regions show no obvious structural change or visible damage after coating, suggesting that the ODPA process does not significantly alter the bond-pad morphology.

Author Contributions: O.C.: Conceptualization, funding acquisition, and manuscript review; S.S.N. and D.K.K.: Methodology, writing—original draft, and data analysis; P.S.A. and K.T.A.T.: Data curation and analysis of optical microscopy, corrosion screening, and RAIRS; D.A.S.P. and S.M.N.: XPS and SEM data curation. All authors have read and agreed to the published version of the manuscript.

Funding: Authors gratefully acknowledge the University of North Texas for the partial support of this work.

Data Availability Statement: The data supporting the findings of this study are available from the corresponding author upon reasonable request.

Acknowledgments: The authors acknowledge NXP Semiconductors for providing wire-bonded devices and Al wafer samples for testing. The authors acknowledge TEL for Cu wafers used in this study. We also extend our gratitude to Kevin Antony Jesu Durai for assistance in setting up the experiments. XPS was collected in part at the University of North Texas's Materials Research Facility, a shared research facility for multi-dimensional fabrication and characterization. SEM imaging was conducted using the shared instrumentation of the University of North Texas Department of Chemistry.

Conflicts of Interest: The authors declare no conflicts of interest. The funders had no role in the design of the study; in the collection, analyses, or interpretation of data; in the writing of the manuscript; or in the decision to publish the results.

Abbreviations

The following abbreviations are used in this manuscript:

PCC-Al	Palladium-coated copper–aluminum
LQFP	Low-Profile Quad Flat Packages
MAPBGA	Mold Array Process Ball Grid Array
ODPA	Octadecylphosphonic acid
IMC	Intermetallic compounds
RAIRS	Reflection–absorption infrared spectroscopy
AFM	Atomic force microscopy
SEM	Scanning electron microscopy
BED	Backscattered electron detector
XPS	X-ray photoelectron spectroscopy

References

1. Zhou, H.; Chang, A.; Fan, J.; Cao, J.; An, B.; Xia, J.; Yao, J.; Cui, X.; Zhang, Y. Copper Wire Bonding: A Review. *Micromachines* **2023**, *14*, 1612. [CrossRef] [PubMed]
2. Harman, G. *Wire Bonding in Microelectronics*, 3rd ed.; McGraw-Hill: New York, NY, USA, 2010.
3. Zhou, H.; Zhang, Y.; Cao, J.; Su, C.; Li, C.; Chang, A.; An, B. Research Progress on Bonding Wire for Microelectronic Packaging. *Micromachines* **2023**, *14*, 432. [CrossRef] [PubMed]

4. Kumaravel, D.K.; Sridharan Nair, S.; Tran, K.T.A.; Ahluwalia, P.; Antony Jesu Durai, K.; Chyan, O. Post Wire-Bonding Corrosion Prevention Strategies to Mitigate Chloride- and Bromide-Induced Corrosion Failures in Cu- and PCC-Based Wire-Bonded Packages. *Micromachines* **2025**, *16*, 1155. [CrossRef] [PubMed]
5. Hang, C.J.; Wang, C.Q.; Mayer, M.; Tian, Y.H.; Zhou, Y.; Wang, H.H. Growth Behavior of Cu/Al Intermetallic Compounds and Cracks in Copper Ball Bonds during Isothermal Aging. *Microelectron. Reliab.* **2008**, *48*, 416–424. [CrossRef]
6. Liu, C.-P.; Chang, S.-J.; Liu, Y.-F.; Su, J. Corrosion-Induced Degradation and Its Mechanism Study of Cu-Al Interface for Cu-Wire Bonding under HAST Conditions. *J. Alloys Compd.* **2020**, *825*, 154046. [CrossRef]
7. Uno, T.; Yamada, T. Improving Humidity Bond Reliability of Copper Bonding Wires. In Proceedings of the IEEE Electronic Components and Technology Conference (ECTC), Las Vegas, NV, USA, 1–4 June 2010. [CrossRef]
8. Mathew, V.; Chopin, S. Corrosion Reliability of Copper Wirebond (CuWB) Packages-Impact of Voltage and Corrosive Ions from Packaging Materials. In Proceedings of the 48th International Symposium on Microelectronics (IMAPS), Orlando, FL, USA, 26–29 October 2015. [CrossRef]
9. Chopin, S.F.; Mathew, V. Controlling Extrinsic Chloride Ions Effect on Copper Wirebond Reliability. In Proceedings of the 52nd International Symposium on Microelectronics (IMAPS 2019), Boston, MA, USA, 30 September–3 October 2019; p. 000095. [CrossRef]
10. Idrac, J.; Mankowski, G.; Thompson, G.; Skeldon, P.; Kihn, Y.; Blanc, C. Galvanic Corrosion of Aluminium-Copper Model Alloys. *Electrochim. Acta* **2007**, *52*, 7626–7633. [CrossRef]
11. Ross, N.; Asokan, M.; Ashok, G.I.A.; Caperton, J.; Alptekin, J.; Salunke, A.S.; Chyan, O.M. Mechanistic Study of Copper Wire-Bonding Failures on Packaging Devices in Acidic Chloride Environments. *Microelectron. Reliab.* **2020**, *113*, 113917. [CrossRef]
12. Li, W.; Liu, K.; Wu, J.; Lian, Q.; Qiang, Y.; Pan, J.; Jin, Y. Numerical Simulation of Carbon Steel Atmospheric Corrosion under Varying Electrolyte-Film Thickness and Corrosion Product Porosity. *NPJ Mater. Degrad.* **2023**, *7*, 3. [CrossRef]
13. Alptekin, J.; Caperton, J.; Kumaravel, D.K.; Asokan, M.; Ashok, G.I.A.; Chyan, O. Exploration of Interfacial Materials Chemistry Control to Improve Cu Wire-Bonding Reliability. *J. Microelectron. Electron. Packag.* **2024**, *21*, 42–49. [CrossRef]
14. Qin, W.; Anderson, T.; Chang, G. Mechanism to Improve the Reliability of Copper Wire Bonding with Palladium-Coating of the Wire. *Microelectron. Reliab.* **2019**, *99*, 239–244. [CrossRef]
15. Qin, I.; Xu, H.; Clauberg, H.; Cathcart, R.; Acoff, V.L.; Chylak, B.; Huynh, C. Wire Bonding of Cu and Pd Coated Cu Wire: Bondability, Reliability, and IMC Formation. In Proceedings of the IEEE Electronic Components and Technology Conference (ECTC), Lake Buena Vista, FL, USA, 31 May–3 June 2011; pp. 1489–1495. [CrossRef]
16. Zeng, Y.; Bai, K.; Jin, H. Thermodynamic Study on the Corrosion Mechanism of Copper Wire Bonding. *Microelectron. Reliab.* **2013**, *53*, 985–1001. [CrossRef]
17. Kumaravel, D.K.; Durai, K.A.J.; Nair, S.M.; Nair, S.S.; Yu, H.H.; Alptekin, J.; Chyan, O.M.R.; Mathew, V. Enhancing Cu Wire-Bonding Reliability by a Cu-Selective Passivation Coating. In Proceedings of the IEEE 74th Electronic Components and Technology Conference (ECTC), Denver, CO, USA, 28–31 May 2024; pp. 1206–1212. [CrossRef]
18. Kumaravel, D.K.; Jesu Durai, K.A.; Nair, S.M.; Tran, K.T.A.; Chyan, O.; Poliah, R.; Chan, M.Z.; Mathew, V. Innovative Cu-Selective Passivation Coatings for Enhanced Reliability in Cu Interconnects for IC Packaging. In Proceedings of the 2024 IEEE 26th Electronics Packaging Technology Conference (EPTC), Singapore, 3–6 December 2024; pp. 534–540. [CrossRef]
19. Paniagua, S.A.; Giordano, A.J.; Smith, O.N.L.; Barlow, S.; Li, H.; Armstrong, N.R.; Pemberton, J.E.; Brédas, J.-L.; Ginger, D.; Marder, S.R. Phosphonic Acids for Interfacial Engineering of Transparent Conductive Oxides. *Chem. Rev.* **2016**, *116*, 7117–7158. [CrossRef] [PubMed]
20. Wan, X.; Lieberman, I.; Asyuda, A.; Resch, S.; Seim, H.; Kirsch, P.; Zharnikov, M. Thermal Stability of Phosphonic Acid Self-Assembled Monolayers on Alumina Substrates. *J. Phys. Chem. C* **2020**, *124*, 2531–2542. [CrossRef]
21. Zhao, R.; Hauert, R.; Crockett, R.; Cancellieri, C.; Gaan, S.; Schmutz, P.; Heuberger, M.P.; Jeurgens, L.P.H. Aqueous Phosphonic Acid Treatments of Aluminium: Effect of Oxide Dissolution and Re-Oxidation on Adsorbate Formation. *Appl. Surf. Sci.* **2024**, *667*, 160363. [CrossRef]
22. Hoque, E.; DeRose, J.A.; Kulik, G.; Hoffmann, P.; Mathieu, H.J.; Bhushan, B. Alkylphosphonate Modified Aluminum Oxide Surfaces. *J. Phys. Chem. B* **2006**, *110*, 10855–10861. [CrossRef] [PubMed]
23. Hoque, E.; DeRose, J.A.; Hoffmann, P.; Bhushan, B.; Mathieu, H.J. Low Adhesion, Non-Wetting Phosphonate Self-Assembled Monolayer Films Formed on Copper Oxide Surfaces. *Ultramicroscopy* **2009**, *109*, 1015–1022. [CrossRef] [PubMed]
24. Pujari, S.P.; Scheres, L.; Marcelis, A.T.M.; Zuilhof, H. Covalent Surface Modification of Oxide Surfaces. *Angew. Chem. Int. Ed.* **2014**, *53*, 6322–6356. [CrossRef] [PubMed]
25. Hoque, E.; DeRose, J.A.; Hoffmann, P.; Mathieu, H.J.; Bhushan, B.; Cichomski, M. Phosphonate Self-Assembled Monolayers on Aluminum Surfaces. *J. Chem. Phys.* **2006**, *124*, 174710. [CrossRef] [PubMed]
26. Seo, Y.I.; Lee, Y.J.; Kim, D.-G.; Lee, K.H.; Kim, Y.D. Mechanism of Aluminum Hydroxide Layer Formation by Surface Modification of Aluminum. *Appl. Surf. Sci.* **2010**, *256*, 4434–4437. [CrossRef]

27. Zhao, W.; Göthelid, M.; Hosseinpour, S.; Johansson, M.B.; Li, G.; Leygraf, C.; Johnson, C.M. The Nature of Self-Assembled Octadecylphosphonic Acid (ODPA) Layers on Copper Substrates. *J. Colloid Interface Sci.* **2021**, *581*, 816–825. [CrossRef] [PubMed]
28. Liakos, I.L.; Newman, R.C.; McAlpine, E.; Alexander, M.R. Study of the Resistance of SAMs on Aluminium to Acidic and Basic Solutions Using Dynamic Contact Angle Measurement. *Langmuir* **2007**, *23*, 995–999. [CrossRef] [PubMed]
29. Luschtinetz, R.; Seifert, G.; Jaehne, E.; Adler, H.J.P. Infrared Spectra of Alkylphosphonic Acid Bound to Aluminium Surfaces. *Macromol. Symp.* **2007**, *254*, 248–253. [CrossRef]
30. Frey, B.L.; Hanken, D.G.; Corn, R.M. Vibrational Spectroscopic Studies of the Attachment Chemistry for Zirconium Phosphonate Multilayers at Gold and Germanium Surfaces. *Langmuir* **1993**, *9*, 1815–1820. [CrossRef]
31. Zenobi, M.C.; Luengo, C.V.; Avena, M.J.; Rueda, E.H. An ATR-FTIR Study of Different Phosphonic Acids in Aqueous Solution. *Spectrochim. Acta A Mol. Biomol. Spectrosc.* **2008**, *70*, 270–276. [CrossRef] [PubMed]
32. Jalili, M.; Rostami, M.; Ramezanzadeh, B. Surface Modification of Aluminum Flakes with Amino Trimethylene Phosphonic Acid: Studying the Surface Characteristics and Corrosion Behavior of the Pigment in the Epoxy Coating. *Corrosion* **2015**, *71*, 628–640. [CrossRef] [PubMed]
33. Wang, S.; Liu, C.; Shan, F.; Qi, G. Amino-Tris-(Methylenephosphonic Acid) Layers Adsorption on AA6061 Aluminum Alloy. *Acta Metall. Sin. Engl. Lett.* **2008**, *21*, 355–361. [CrossRef]
34. Xia, D.-H.; Pan, C.; Qin, Z.; Fan, B.; Song, S.; Jin, W.; Hu, W. Covalent Surface Modification of LY12 Aluminum Alloy Surface by Self-Assembly Dodecyl Phosphate Film towards Corrosion Protection. *Prog. Org. Coat.* **2020**, *143*, 105638. [CrossRef]
35. Adolphi, B.; Jähne, E.; Busch, G.; Cai, X. Characterization of the Adsorption of ω-(Thiophene-3-yl Alkyl) Phosphonic Acid on Metal Oxides with AR-XPS. *Anal. Bioanal. Chem.* **2004**, *379*, 646–652. [CrossRef] [PubMed]
36. Zhao, R.; Rupper, P.; Gaan, S. Recent Development in Phosphonic Acid-Based Organic Coatings on Aluminum. *Coatings* **2017**, *7*, 133. [CrossRef]
37. Textor, M.; Ruiz, L.; Hofer, R.; Rossi, A.; Feldman, K.; Hähner, G.; Spencer, N.D. Structural Chemistry of Self-Assembled Monolayers of Octadecylphosphoric Acid on Tantalum Oxide Surfaces. *Langmuir* **2000**, *16*, 3257–3271. [CrossRef]
38. Kalinovych, V.; Saeedur Rahman, M.; Piliai, L.; Kosto, Y.; Mehl, S.L.; Skála, T.; Matolínová, I.; Matolín, V.; Prince, K.C.; Xu, Y.; et al. Thermal Stability and Protective Properties of Phenylphosphonic Acid on Cu(111). *Appl. Surf. Sci.* **2022**, *600*, 154036. [CrossRef]
39. Hofer, R.; Textor, M.; Spencer, N.D. Alkyl Phosphate Monolayers, Self-Assembled from Aqueous Solution onto Metal Oxide Surfaces. *Langmuir* **2001**, *17*, 4014–4020. [CrossRef]
40. Gouzman, I.; Dubey, M.; Carolus, M.D.; Schwartz, J.; Bernasek, S.L. Monolayer vs. Multilayer Self-Assembled Alkylphosphonate Films: X-Ray Photoelectron Spectroscopy Studies. *Surf. Sci.* **2006**, *600*, 773–781. [CrossRef]
41. Kumar, G.I.A.; Alptekin, J.; Caperton, J.; Salunke, A.; Chyan, O. Accelerated Reliability Testing of Cu-Al Bimetallic Contact by a Micropattern Corrosion Testing Platform for Wire Bond Device Application. *MethodsX* **2021**, *8*, 101320. [CrossRef] [PubMed]

Disclaimer/Publisher's Note: The statements, opinions and data contained in all publications are solely those of the individual author(s) and contributor(s) and not of MDPI and/or the editor(s). MDPI and/or the editor(s) disclaim responsibility for any injury to people or property resulting from any ideas, methods, instructions or products referred to in the content.